Polarized spectral emittance from periodic micromachined surfaces. I. Doped silicon: The normal direction

Peter J. Hesketh* and Jay N. Zemel
Department of Electrical Engineering and Center for Sensor Technologies, University of Pennsylvania, Philadelphia, Pennsylvania 19104-6390

Benjamin Gebhart
Department of Mechanical Engineering and Applied Mechanics, University of Pennsylvania, Philadelphia, Pennsylvania 19104-6390

(Received 27 February 1987; revised manuscript received 16 February 1988)

The normal, polarized spectral ($3\ \mu\text{m} \leq \lambda \leq 14\ \mu\text{m}$) emittances of highly doped, micromachined, periodic structures on heavily phosphorus-doped (110) silicon ($[P] \sim 5\times10^{19}\ \text{cm}^{-3}$) were measured for pattern repeat scales, Λ, of 10, 14, 18, and 22 μm and depths ranging from 0.7 to 45 μm. These structures have dimensions that are comparable to the wavelengths of the measured radiation. The *s*-polarization vector in these measurements was perpendicular to the grating vector. The data demonstrated that the emittance from the deep structures is dominated by standing (quantized) electromagnetic waves in a direction normal to the surface similar to those in an organ pipe. Wood's singularities were clearly visible in the *p*-polarized emission on shallow gratings (depth $\leq 1.5\ \mu$m). It is concluded that these measurements, particularly the *s*-polarized emission from deep gratings, cannot be explained by calculations of electromagnetic singularities on lamellar gratings.

I. INTRODUCTION

Radiant energy from heated bodies is a classic topic in both science and technology. The accounting of the spectral distribution of blackbody radiation from macroscopic structures created the intellectual ferment that led to the quantum theory.[1] Inherent in both the measurements and the theoretical model is the assumption that the geometric scale of the radiators, S, is substantially larger than the wavelength λ being measured. This was a natural assumption given the available methods for fabricating the radiating structures. The planar photolithographic manufacturing technology that has evolved in the microelectronics industry now makes it possible to study the region where $S \approx \lambda$. In this and the accompanying paper, new experimental evidence is presented which demonstrates that the emissive properties of a moderately conducting surface (heavily doped Si) are profoundly altered when it is composed of structures where $S \sim \lambda$.[2] The surface containing these small-scale structures will be referred to as microconfigured (MC) surfaces.

An earlier paper reported that the polarized spectral emittance in the normal direction from deep gratings in heavily doped Si with $H = 47\pm6\ \mu$m was not only greatly enhanced over that of smooth silicon, there were also pronounced spectral-emission maxima suggestive of a path difference or standing-wave phenomena.[3] When the wave number

$$k_{\max}(m) = \frac{1}{\lambda_{\max}(m)} ,$$

corresponding to the wavelength of the emittance maxima $e_n^{\max}(\lambda_{\max}, p_i, 400\,^\circ\text{C})$, was plotted against a sequence of integers m a linear relation was obtained whose slope was independent of the grating repeat distance Λ. Four types of periodic structures with $\Lambda = 10$, 14, 18, and 22 μm were examined. The maxima were associated with the existence of discrete electromagnetic standing waves or modes in the slots of the gratings using the simple relation

$$k_{\max}(m) = \frac{2m+1}{4H} . \tag{1}$$

The values of H obtained from the rms value for the slope were found to be $H = 40\pm5\ \mu$m for both *s* and *p* polarizations. This was in excellent agreement with the average measured depth of $47\pm8\ \mu$m for all of the gratings. It was concluded that the observed maxima in the emittances arise from resonances associated with the vertical standing electromagnetic waves or normal modes in the microslots. These are "organ-pipe" modes using a simple acoustic analogy.[3] These allowed standing waves are the source of the radiation density of states used in the derivation of Planck's radiation law.[1,4] The electromagnetic standing waves also closely resemble waveguide modes where the TE mode corresponds to the *s*-polarized emission and the TM mode to *p*-polarized emission.

Additional data are presented here confirming this explanation. Because of the dimensional scale of the MC, the continuum model used to derive the radiation density of states $g_r(\nu)$ can no longer be used. Instead, the discrete summation form of $g_r(\nu)$ has to be used to determine the blackbody-radiation law. The importance of this type of behavior was examined theoretically by Baltes and co-workers in their study of the Weyl problem.[5–9] When S for the cavity becomes comparable to the λ of the emitted radiation, the approximation that the density of states for the electromagnetic normal modes is a continuous function of frequency no longer applies.[4] Baltes *et al.* have demonstrated that the mode density in a rectilinear parallelepiped cavity is reduced by a factor of 30% when the linear dimensions are equal to the wavelength and the mode structure is polarization dependent.[7,8]

As will be shown, the results presented here and in the accompanying paper suggest that it is possible to examine the structure of $g_r(\nu)$ and the properties of individual electromagnetic cavity modes in the MC surfaces in some detail by means of the directional spectral polarized emittance. No attempt is made to compare these experimental data to a vector electromagnetic theory for several reasons. Because a thorough theoretical treatment of the deep-grating, finite-wall conductivity problem is not available, treating this problem is beyond the scope of these papers. Such theory as exists on resonances in deep gratings fails to account for some of the key observations obtained. On this last point, Wirgin and Maradudin have given a theoretical discussion of the resonant enhancement of *s*-polarized radiation in lamellar gratings that may be treated as a limiting case for the results given in these papers.[10] In the specific case they treat, no far-field resonances are possible, i.e., all of the incident energy is thrown into the specular order. Assuming that scaling to the micrometer dimensions treated in this and the succeding paper is valid, it is straightforward to show that their case corresponds to a $\Lambda = 10$ μm grating, with a slot width $W = 9.2$ μm and a depth of $H = 26$ μm. This is not too far from the $\Lambda = 10$ μm grating with $W = 8.4$ μm and $H = 14$ μm to be discussed below. A pronounced *s*-polarized resonance is observed specifically in the long-wavelength regime where diffraction theory implies there should be none. By contrast, if it is assumed that this is a result of a standing wave in the cavity, a reasonable if not rigorous explanation is available. Given that the experimental data indicate that processes other than those suggested by conventional diffraction theory are operative, it is desirable to present sufficient information to assist future experimental and theoretical studies.

Thermal radiant emission from MC surfaces is just one aspect of the broader, largely unexplored matter of heat-transfer processes involving structures with S in the micrometer and submicrometer regime. The nature of the interactions when the characteristic scale of the physical heat-transfer process becomes comparable to S is a fertile area of future research. The one case where an immense amount of research has been done is the interaction of electromagnetic radiation with shallow gratings or narrow slits.[11,12] In the case of gratings, S is generally the magnitude of the grating repeat vector, $|\Lambda| = \Lambda$. A shallow grating is one where the depth of the grating groove or slot, H, is much less than Λ. Correspondingly, a deep grating will be one where $H > \Lambda$. To the best of our knowledge, no studies have been reported on periodic microconfigured surfaces.

The specimens used in these investigations were micromachined in (110) lightly doped silicon wafers using current photolithographic and crystallographically selective wet etches.[13–15] Following the etching, the wafers were heavily doped using standard diffusion technology.[16,17] Two classes of surface structure were prepared and studied: lamellar gratings and arrays of microcavities.

Because Kirchhof's law requires that the absorption equal the emission, emittance measurements provide a simple and direct way to explore the influence of MC surface structures on the absorption of electromagnetic energy.[18,19] Scattering and absorption of electromagnetic energy from randomly roughened surfaces, and particles when $S \sim \lambda$ is an important area of current research,[20] including surface-enhanced Raman scattering (SERS),[21,22] the resonant growth of metal gratings.[23] The failure of classical emission theory from macroscopic structures to account for the observations to be presented is discussed elsewhere.[24,25] There is a long list of topics that would benefit from a better understanding of electromagnetic interactions when $S \sim \lambda$ ranging from radar[26] to atmospheric and astronomical studies.[27,28]

II. EXPERIMENTAL PROCEDURES

Single-crystal, Czochralski-grown, (110)-oriented, 25–60-Ω cm p-type wafers, 0.25–0.30 mm thick were chosen as the sample substrates for two reasons: the crystallographic etching characteristics simplified the manufacture of the specimens, and the ease of preparing heavily doped materials with near-metallic properties. One side of the wafer was polished and the other was rough cut. The mask set for the samples was designed to contain four different MC structures each covering a 1×1 cm^2 area. The individual structures consisted of a $W \times W$ square, two rectangular structures of $W \times 50$ μm and $W \times 100$ μm, and a grating with a slot width of W. The repeat distances, Λ, were 10, 14, 18, and 22 μm, i.e., the same as is Ref. 3. The fabrication process was quite standard. A 1.2-μm wet oxide was grown at 1100 °C as the field oxide. Appropriate windows were opened in the oxide and the MC elements were produced using a 40 wt. % aqueous solution of KOH at 52 °C for the crystallographically selective etch. Once the MC structures were produced on the wafers, both sides were phosphorus doped using a spin-on dopant at 1250 °C for up to 5 h. To ensure that the radiator side of the wafer was heavily doped, the procedure was repeated several times for a total exposure of 15–16 h. Spreading resistance measurements demonstrated that the emitting surface had a 20-μm-thick doped layer with a carrier concentration in the $(0.8-1.6) \times 10^{20}$ cm^3 range. The accuracy of these numbers is $\pm 25\%$. Auger measurements on selected samples indicated that the phosphorus concentration was within this uncertainty. The diffused layer on the opposite side of the specimen served as an integrated heater element. The heater was covered by a 400-nm-thick oxide layer for isolation and was contacted through appropriate windows and a deposited Au-Cr layer by 75-μm-thick copper wires attached with a silver, high-temperature epoxy. A schematic drawing of the sample is shown in Fig. 1. Care was taken to remove excess oxide from the emitting surface by removing the initial oxides with an HF etch and

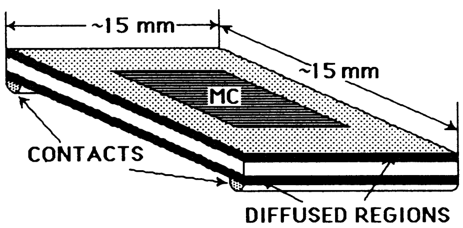

FIG. 1. Schematic drawing of the integrated microconfigured emittance sample.

subsequently giving the surface a light HF etch prior to each measurement.

The cross section of the MC structures arising from the KOH crystallographic etch are not simple. The square mask led to the formation of hexagonal cavities while the two rectangular masks produced wedge-shaped cavities bounded by {111} planes. The grating slots had reasonably straight {111} side walls with {100} planes forming a wedge at the bottom of the slots. Schematic perspective drawings of the MC structures are shown in Fig. 2. The various angles employed and the polarization vectors are illustrated in Fig. 2(c).

The layout of the experiment is illustrated in Fig. 3. The measurements reported in this paper were all conducted in the normal direction, i.e., polar angle $\theta=0°$. The HeNe laser was used to assist the focusing of the radiation from the specimen onto the slits of the spectrometer. The temperature of the sample was measured with fine thermocouples in contact with the integrated heater on the back of the sample. These thermocouples provided the input signal to a control circuit for the sample heater current that was referenced against a thermocouple in intimate contact with the blackbody reference source. The sample holder was designed to minimize conductive and convective heat losses and, as a result, close to uniform radiant emission occurred. The heater dissipated approximately 4 W. The samples were held in a temperature range from $300\,°\mathrm{C} \leq T \leq 400\,°\mathrm{C}$ by controlling against a blackbody source at a corresponding temperature T. Temperature fluctuations were typically less than 0.2 °C during the course of a measurement. Any systematic error arising from temperature differences between the sample and the monitoring thermocouples would produce a wavelength error that is greater at shorter wavelengths. Calculations based on an assumed temperature fluctuation of 1 °C indicated that the maximum error in the measured emittance would be of the order of 1%. The flux of radiation emitted normal to the MC surface was passed through an infrared polarizer and was then analyzed in a NaCl prism spectrometer with a HgCdTe infrared detector. The wavelength regime measured in all data presented here is $3\ \mu\mathrm{m} \leq \lambda \leq 14\ \mu\mathrm{m}$.

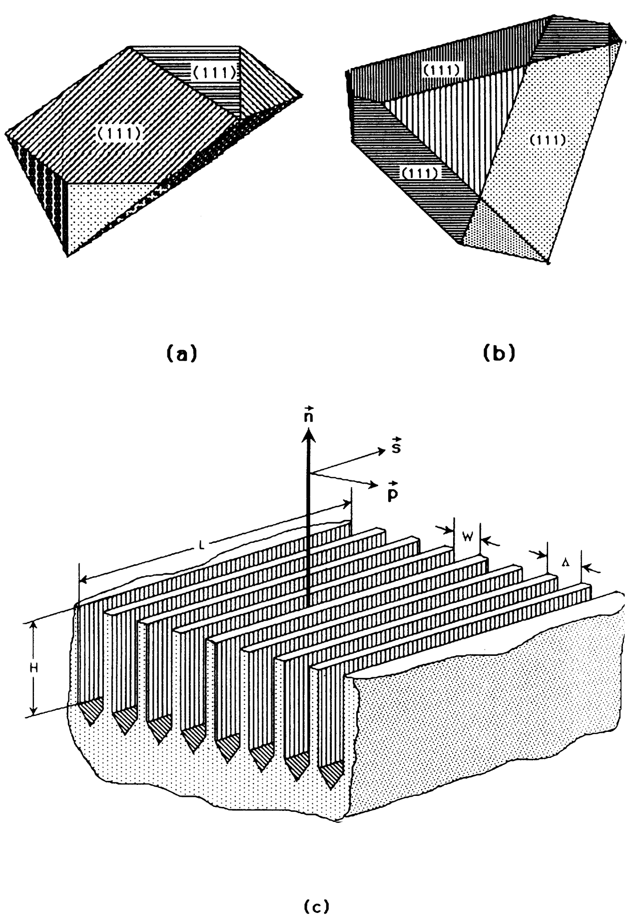

FIG. 2. Schematic drawings of three types of microconfigures surfaces. (a) "Hexagonal" cavities from square apertures; (b) schematic drawing of a rectangular "wedge" arising from rectangular apertures; (c) schematic drawing of the "deep" grating showing the orientation of the s- and p-polarization vectors relative to Λ. Also shown are the various characteristic geometric lengths defined in the text.

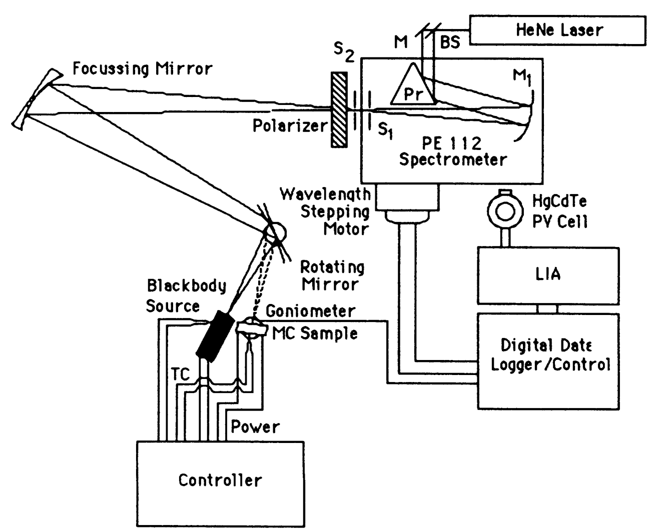

FIG. 3. Schematic layout of the emittance measuring equipment: TC, thermocouple; S, slit; M, flat mirror; M_1, parabolic mirror; BS, beam splitter; PV, photovoltaic detector; PE, Perkin-Elmer, and LIA, lock-in amplifier, PR, NaCl prism; MC, microconfigured sample.

The polarized normal ($\theta=0°$) spectral emittance $e_n(\lambda,p_i,T)$ was obtained by first measuring the polarized spectral intensity $I_{S,n}(\lambda,p_i,T)$ and storing it in the logging system. The orientation of the polarization vectors, $p_i=s,p$, are shown in Fig. 2(c). The radiant flux from the blackbody, $I_{b,n}(\lambda,p_i,T)$, was also measured at normal incidence and stored. Finally, the background polarized spectral intensity $I_{a,n}(\lambda,p_i,T)$ was measured and stored. The emittance was then computed using the relation

$$e_n(\lambda,p_i,T)=\frac{[I_{S,n}(\lambda,p_i,T)-I_{a,n}(\lambda,p_i,T)]}{[I_{b,n}(\lambda,p_i,T)-I_{a,n}(\lambda,p_i,T)]} . \quad (2)$$

Reproducible data were obtained in this way due to the stability of the thermal controls on the blackbody source and the stability of the sample relative to the blackbody temperature. A more detailed description of the sample fabrication, their characteristics, and the experimental procedures may be found in Ref. 25.

III. RESULTS

The experimental results are divided into three sections: "deep" gratings with $\Lambda/H\leq 1$; shallow gratings with $\Lambda/H>1$; microcavities. From Fig. 2(c), rotation of the plane of observation relative to Λ, i.e., the azimuthal angle ϕ for $\theta=0°$ has two effects. It exchanges the definition of the s and p polarizations and offers a different area of the sample for observation. In other words, at $\theta=0°$, $s(\phi=90°)\equiv p(\phi=0°)$ and $s(\phi=0°)\equiv p(\phi=90°)$. As a consequence, data for either $\phi=0°$ or 90° were employed depending on which orientation had the optimum signal-to-noise ratio. In general, the data for the two values of ϕ were equal to within 5%, indicating very good sample uniformity. A number of $e_n(\lambda,p_i,T)$ measurements were carried out in the range $300\,°C\leq T\leq 400\,°C$. Both $k_{\max}(m)$ and $e_n^{\max}(\lambda_{\max},p_i, 300\,°C\leq T\leq 400\,°C)$ were found to be independent of temperature.

A. Deep gratings

As pointed out in the Introduction, preliminary data on deep grating have been published elsewhere.[3] Data demonstrating that standing-wave modes are present even in gratings as shallow as $H=7\ \mu m$ are presented in Fig. 4 for $\Lambda=10$, 14, 18, and 22 μm, and in Fig. 5 for

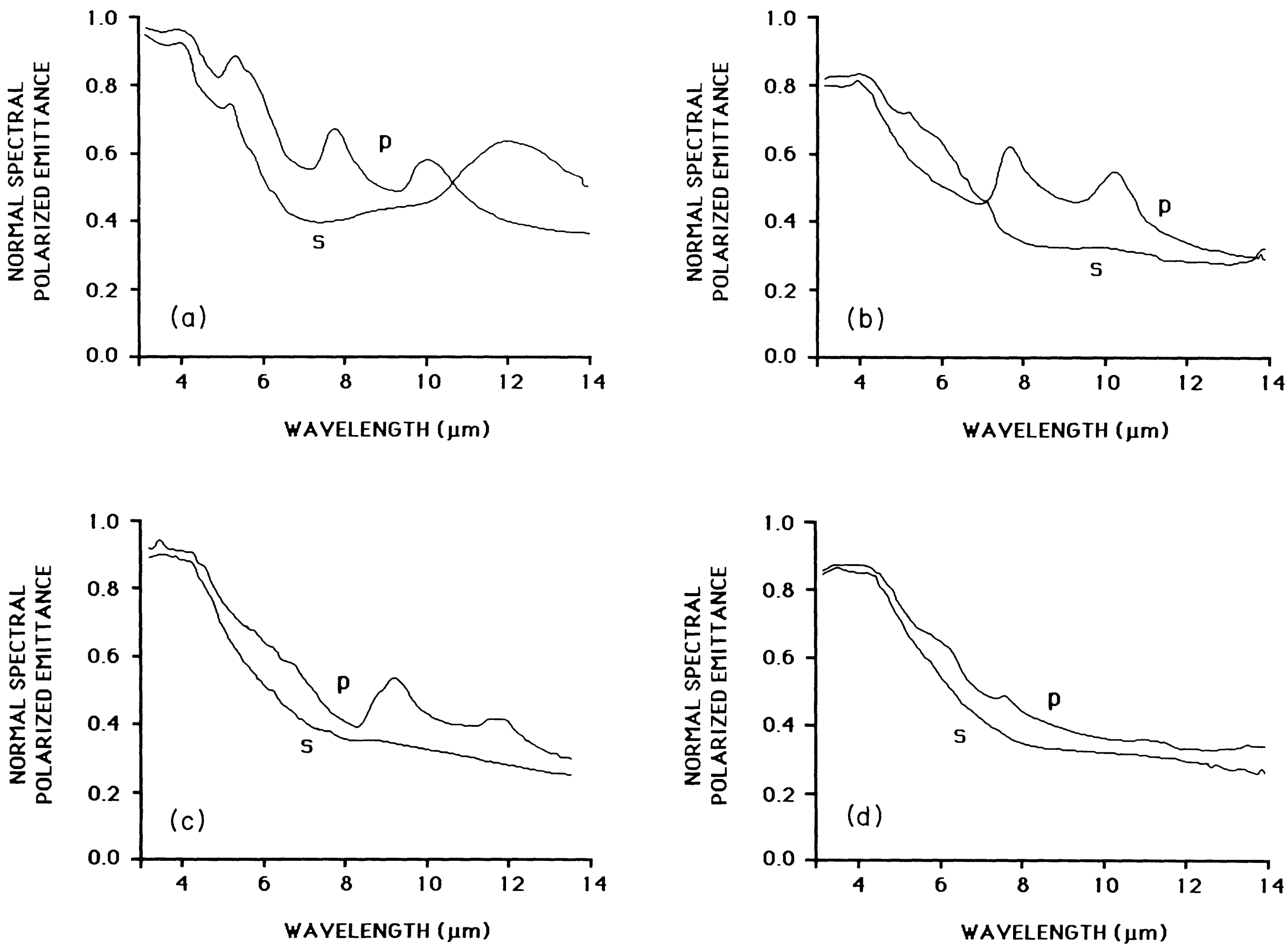

FIG. 4. Normal spectral polarized emittance of "deep" silicon gratings at $T=400\,°C$: (a) $\Lambda=10\ \mu m$, $H=7\ \mu m$, $W=7.3\ \mu m$; (b) $\Lambda=14$, $H=7\ \mu m$, $W=8.4\ \mu m$; (c) $\Lambda=18\ \mu m$, $H=7\ \mu m$, $L=12.6\ \mu m$; (d) $\Lambda=22\ \mu m$, $H=7\ \mu m$, $L=14\ \mu m$.

$H \approx 14$ μm, $\Lambda = 10$ and 22 μm. $k_{max}(m)$ obtained from the data in Figs. 4 and 5 as well as other data for $H = 35$ μm are plotted in Fig. 6. The rms values of H calculated from the slopes of the various $k_{max}(m)$ are 6.6, 14.9, 28.8, and 32.2 μm, respectively. The accuracy of the measured depths and the slopes from Fig. 6 is approximately $\pm 10\%$. In view of the experimental uncertainty, the agreement is quite satisfactory. The resonant behavior occurs even when H becomes comparable to the wavelengths of the emitted radiation. On closer examination of the data presented in Ref. 3, it was noted that what had appeared to be a single continuous line for the $k_{max}(m)$ for $\Lambda = 10$ μm, $H = 47$ μm, was in fact two discontinuous lines with different slopes for each polarization. Curiously, linear regressions with these two slopes appeared in both polarizations. This is shown in Fig. 7. In general, the linearity of the data and the respectable agreement between the measured depths and the values derived from Eq. (1) are strong additional confirmatory evidence for the proposed model, despite the number of data points being sparse for some geometries.

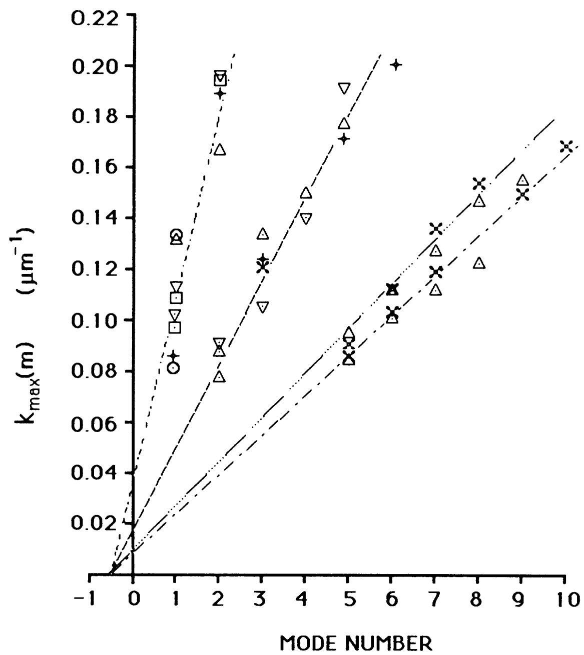

FIG. 6. Wave number of normal spectral (s and p) polarized emittance maxima. $k_{max}(m)$ as a function of order m for $7 \leq H < 44$ μm from silicon gratings: s polarized, $\Lambda = 22$ μm ($\times$); $\Lambda = 10$ μm ($+$); p polarized, $\Lambda = 22$ μm ($\triangle$); $\Lambda = 18$ μm ($\odot$); $\Lambda = 14$ μm ($\boxdot$); $\Lambda = 10$ μm (∇).

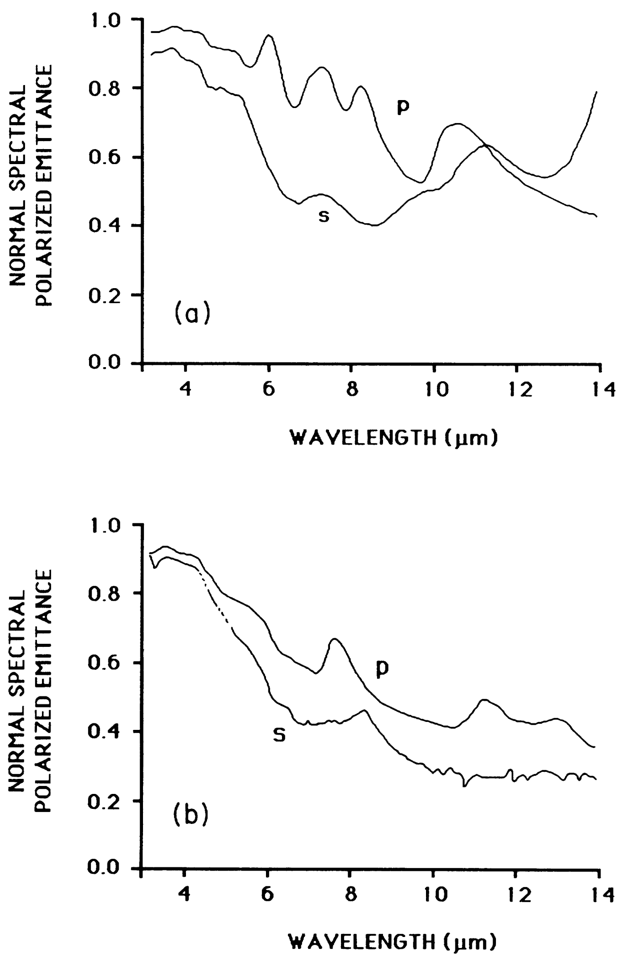

FIG. 5. Normal spectral polarized emittance of "deep" silicon gratings at $T = 400$ °C: (a) $\Lambda = 10$ μm, $H = 14$ μm, $W = 7.3$ μm; (b) $\Lambda = 22$ μm, $H = 13$ μm, $L = 14$ μm.

It was observed in all data taken that the averaged p-polarized spectral emittance (i.e., ignoring the modal maxima) decreased monotonically with λ. This was not always the case for the averaged s-polarized spectral emittance. When $\lambda \geq \Lambda$, the emittance would either decrease more slowly with λ or would actually increase. A crossover was observed at 9 μm in the $\Lambda = 10$ μm data, and at $\lambda = 10.5$ μm in the $\Lambda = 14$ μm data for $H = 47 \pm 6$ μm in Ref. 3. Similar behavior may be seen in Fig. 4(a) at $\lambda \approx 10$ μm, $H = 7$ μm, at $\lambda \approx 14$ μm, $H = 7$ μm in Fig.

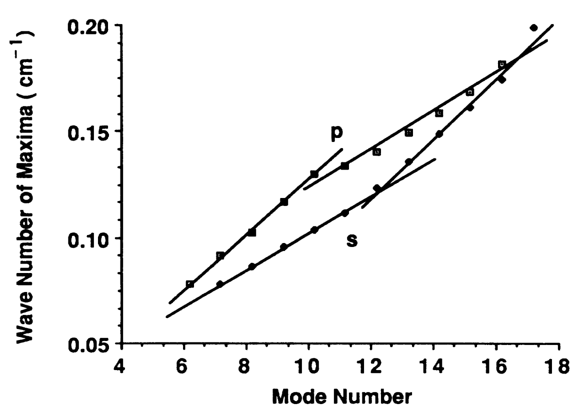

FIG. 7. Wave number of normal spectral polarized emittance maxima. $k_{max}(m)$ as a function of order m, from silicon gratings for $\Lambda = 10$ μm and $H \approx 47$ μm.

5(b), and at $\lambda \approx 10$ μm, $H=14$ μm in Fig. 6(a). The absence of this increase in the s-polarized emittance is apparent in Figs. 4(c), 4(d), and 5(b). The standing-wave-induced maxima are more pronounced in the data shown in Fig. 5, corresponding to an $H \approx 14$ μm. The fact that the s-polarized emission becomes larger than the p-polarized emission is a gross departure from the classical behavior of a strictly geometric model.[23,24]

B. Shallow grating

The data presented in this section are limited to a single Λ value of 10 μm, and depths H of 0.7, 1.5, and 3 μm. The data for the three different depths are presented in Fig. 8. The s-polarized emission for $H=0.7$ and 1.5 μm resembles that of the smooth surface. A maximum appears at $\lambda=10.7$ μm, when $H=3$ μm. This increase in emission, for λ greater than Λ, was also observed in Figs. 4(a), 4(b), and 5(a).

The p-polarized emission has a single maximum at $\lambda=5.5$ μm and a double peak at 10 μm. These maxima are independent of H. An additional peak is observed at $\lambda=12.8$ μm in the $H=3$ μm data. These maxima are independent of depth in the p-polarization, suggesting that this behavior is associated with the well-known Wood's singularity.[29] The relationship among wavelength, grating repeat distance, and order of a Wood's singularity at normal incidence is given by

$$\lambda_{\max}=\frac{\Lambda}{m}\frac{\epsilon_1(\lambda)}{[1+\epsilon_1(\lambda)]} \tag{3}$$

where $\epsilon_1(\lambda)$ is the real part of the dielectric constant obtained from free-carrier absorption theory.[30] The necessary parameters were obtained from the measured surface doping level and by correcting published room temperature material constants for the higher temperatures of these emittance measurements. The values chosen were $\tau=1.06\times10^{-14}$ sec and $m^*=0.26$.[31] The real part of the dielectric constant calculated at the peak wavelengths was $\epsilon_1(\lambda=6\ \mu\text{m})=-6.7$ and $\epsilon_1(\lambda=10\ \mu\text{m})=-22.1$. Substituting these values into Eq. (3) for $\Lambda=10$ μm for $m=1$ yields $\lambda_{\max}=10$ μm. For $m=2$ the value is $\lambda=5.9$ μm.

These results are in excellent agreement with the observed maxima. However, we have no explanation for the splitting of the 10-μm line. Since the wavelengths of two of the normal emittance peaks match those calculated for the first- and second-order Wood's singularity of $\theta=0°$, it is concluded that emission is taking place due to a coupling of the surface plasmon to a radiating electromagnetic wave through the grating's periodicity. This would occur when the component of the radiation wave vector in the plane of the grating is equal to the surface plasmon wave vector plus the effective grating wave vector. (See *Note added in proof.*)

C. Microcavities

Two types were studied, rectangular microcavities 8.5 times longer than wide, and "hexagonal" microcavities. The schematic drawings of Figs. 2(a) and 2(b) illustrate the geometry of these structures. The important difference between the gratings and rectangular microcavities is that the rectangular microcavity has a sloping side wall produced by the {111} planes while the gratings have approximate rectangular cross section. Therefore, the type of vertical standing wave associated with the

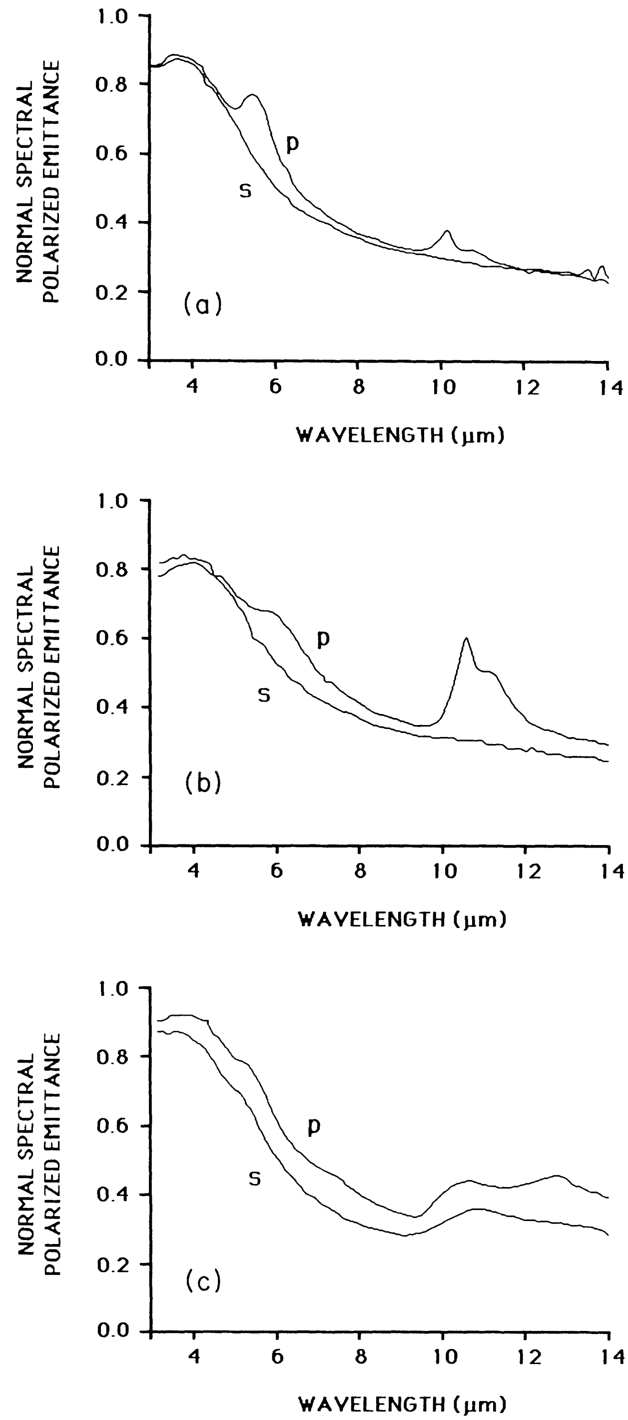

FIG. 8. Normal spectral polarized emittance of "shallow" silicon gratings at $T=400\,°\text{C}$, $\Lambda=10$ μm; (a) $H=0.7$ μm, $W=6.3$ μm; (b) $H=1.5$ μm, $W=7.3$ μm; (c) $H=3$ μm, $W=7.3$ μm.

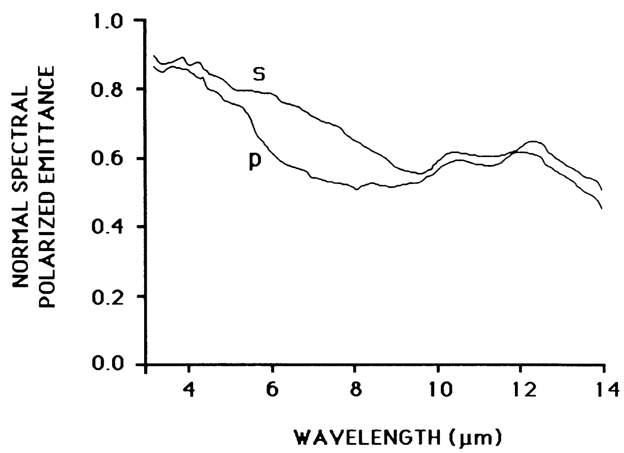

FIG. 9. Normal spectral polarized emittance of "rectangular" silicon cavities at $T=400\,^{\circ}\mathrm{C}$, $\Lambda=10\ \mu\mathrm{m}$, $H=24\ \mu\mathrm{m}$, $W=7.3\ \mu\mathrm{m}$, $L=47\ \mu\mathrm{m}$, and $\phi=0^{\circ}$

electromagnetic modes in the gratings cannot arise in the rectangular microcavities. Only a limited number of measurements were made because these MC structures were soon found to exhibit relatively few resonant features.

The hexagonal microcavities [illustrated in Fig. 2(a)] studied had a repeat distance of 22 μm. Their $e_n(\lambda, p_i, T)$ data were indistinguishable from that of the smooth surface. No other repeat distances were investigated. It should be noted that the "effective" surface area is not changed appreciably by the presence of the microcavities.

In the case of the rectangular microcavities [illustrated in Fig. 2(b)] only the $\Lambda=10$ and 22 μm were investigated. The $\Lambda=22$ μm data showed some diffuse structure similar to that in Fig. 5(d). However, more structure was observed on rectangular microcavities with $L=47$ μm, $\Lambda=10$ μm as shown in Fig. 9. These triangular cavities had a depth of 24 μm. The relevant information in this figure is that the s-polarized emission rises with increasing wavelength when $\lambda \geq \Lambda$ as with the gratings.

IV. DISCUSSION

The data presented here confirm the presence of regularly spaced maxima in the normal spectral emittance of deep, heavily doped silicon gratings. Their spectral position can be accounted for by the presence of vertical standing waves. The maxima are independent of grating repeat distance and of polarization for slots with $H \leq 42$ μm. Although a very simple model is proposed here, it appears to account for much of what has been observed. As will be shown in the accompanying paper, the angular dependence of the polarized spectral emittance provides still further confirmatory information on this proposed model.

The model does not offer detailed insight into how the material and geometric properties of MC structures influence the magnitude of polarized spectral emission from the quantized modes. The increased s-polarized emission observed whenever $\lambda \geq \Lambda$ suggest that the $m=0$ mode is a very effective radiator for this polarization.

The data in Fig. 7 are particularly intriguing. The presence of two slopes for $k_{\max}(m)$ corresponding to $H=39$ μm and ≈ 56 μm suggests that a splitting occurs. One explanation for this behavior is that coupling between the adjacent microslots may occur at smaller Λ because of the thinner walls, ~ 2.7 μm, separating the $\Lambda=10$-μm microslots. This wall thickness approaches the dimensions of the skin depth, ~ 0.5 μm, calculated from the measured dopant density and the effective mass obtained from the literature.[15,32] The data presented here make it clear that the electromagnetic interaction between the resonant states in the cavity and the silicon substrate is quite strong. This is expected from a general consideration of the relationship between thermal noise and blackbody radiation.[33] The spectral emissivity of deep $\Lambda=10$ μm gratings has maximum values that are very close to unity despite the presence of a groove due to the intersection of two {111} planes at the bottom of the microslot. If the coupling between the slots is as strong as may be inferred from Fig. 7, then the character of the blackbody radiation from these slots may demonstrate significant spatial coherence. Further studies of this behavior would be desirable.

Another important issue that will need further examination is the influence of the detailed MC geometry on the density and character of the allowed propagating modes. Variations in the dimensions of the cavity are inevitable no matter which type of etch process is employed. As a result, these geometric variations may introduce an effective "linewidth" for the resonant state. A similar behavior may be expected from the fluctuations in the doping concentration (and the resultant plasmon frequency and skin depth). Geist has commented that one would expect spectral broadening of the resonant modes as a result of the open-ended character of the microslot.[34]

As is well known, the spectral emission from a blackbody is given by Planck's law provided that the linear dimensions of the cavity S are much greater than wavelength λ. Baltes and co-workers extended the derivation of Planck's law to closed cavities in the region where $\lambda \approx S$, under the assumption that the walls were perfectly conducting.[5–8] These boundary conditions assured that the mode density of states would be a noncontinuum function, actually one with δ-function-like properties. Because the density of electromagnetic modes in the deep grooves are restricted by the surface geometry, it is possible to observe directly the discrete modes. For a closed cavity, these authors found that the number of TE and TM modes are no longer the same. They may differ by a factor of 30% or more.[6] This is because of the difference in the boundary conditions for the TE and TM modes. It is interesting to note that the spectral positions of the s- and p-polarized emittance observed the maxima are not the same. However, once the complications of an open-ended cavity and nonperfectly conducting walls are added, the theoretical problem becomes daunting and further experimental study is desirable.

For the measurements reported here, the emittance maxima at the resonance condition are well above the emittance predicted by a classical calculation, i.e., from geometric optics.[24] The maxima occur because of the coupling of resonant cavity modes to radiation modes. At the resonant wavelength, the microslots are, in effect, a more efficient antenna. Thus, a geometric model fails to predict any of the noncontinuum and quantum effects. However, it has correctly predicted the relative values of the s-and p-polarized normal emittance for the widest repeat distance of 22 μm.[24,25]

The Wood's singularities arise from a surface plasmon coupling to a radiating wave through the grating effective wave vector. This arises in the normal p-polarized emittance of $60^\circ \leq \phi \leq 90^\circ$ and in the s-polarized emittance at $\phi = 0^\circ$. The peaks associated with the Wood's singularity are clearly observed in the radiant flux from shallow gratings and become masked by the organ-pipe resonant peaks in the deeper gratings. Theory predicts a single maxima at a wavelength of 10 μm. The double peak is not understood. This appears to be the first time that Wood's singularities have been observed in emission.

The rectangular microcavities also exhibit many of the features that appear with the gratings. The organ-pipe resonances appear to be absent but the Wood's singularity does occur.

In summary, the measurements presented here provide additional substantive confirmation of the influence of standing electromagnetic modes on the blackbody emission from MC surfaces. The data clearly indicate the role of geometry on the emission process. It also provides a basis for obtaining a clearer understanding of emissive (absorptive) processes on both random and irregular, periodic rough surfaces.

Note added in proof. Neviere presents the results of a calculation that demonstrates that the type of variation illustrated in Fig. 8 is due to variations in the poles and zeros of the emitted intensity [M. Neviere, in *Electromagnetic Theory of Gratings,* edited by R. Petit (Springer-Verlag, Berlin, 1980), p. 136].

ACKNOWLEDGMENTS

The authors wish to acknowledge the following: Judson Infrared, Montgomeryville, PA, for their contribution of the HgCdTe infrared detector; Dr. A. Ipri of the RCA Sarnoff Laboratory for supplying the photomasks; Dr. Anatoly Feygenson of the AT&T Bell Laboratories, Reading, PA, for the spreading resistance measurements; the partial support of the EEMS program of the National Science Foundation, D. Silversmith, Program Manager, under Grant No. ECS-84-12241 (P.H. and J.N.Z.); support from the National Science Foundation Grant No. CBT 84-18517 (B.G.); useful discussions with Professor H. Baltes and Professor A. Maradudin (J.N.Z. and P.J.H.).

---

*Now at SRI International, Menlo Park, CA 94025.

[1]M. Planck, *Theory of Heat Radiation* (Dover, New York, 1959) [English translation of *Theorie der Warmestrahlung,* 2nd ed. (J. A. Barth, Leipzig, 1913).

[2]P. J. Hesketh, J. N. Zemel, and B. Gebhart, following paper, Phys. Rev. B **37**, 10 803 (1988).

[3]P. J. Hesketh, J. N. Zemel, and B. Gebhart, Nature (London) **324**, 549 (1986).

[4]R. Loudon, *The Quantum Theory of Light* (Clarendon, Oxford, 1981).

[5]H. P. Baltes and E. R. Hilf, *Spectra of Finite Systems* (Bibliographische Institute-Wissenschaftsverlag, Zurich, 1976).

[6]H. P. Baltes and F. K. Knuebuhl, Helv. Phys. Acta **45**, 481 (1972).

[7]H. P. Baltes, Infrared Phys. **16**, 1 (1976).

[8]R. F. D. Turner, W. A. G. Voss, W. R. Tinga, and H. P. Baltes, J. Microwave Power **19**, 199 (1984).

[9]R. F. D. Turner, W. A. G. Voss, W. R. Tinga, and H. P. Baltes, IEEE Proc. H **132**, 82 (1985).

[10]A. Wirgin and A. A. Maradudin, Phys. Rev. B **31**, 5573 (1985).

[11]M. Born and E. Wolf, *Principles of Optics,* 6th ed. (Pergamon, New York, 1984), p. 401.

[12]R. Petit, in *Electromagnetic Theory of Gratings,* edited by R. Petit (Springer-Verlag, Berlin, 1980), p. 31.

[13]K. E. Bean, IEEE Trans. Electron. Devices **ED-25**, 1185 (1978).

[14]E. Bassous, IEEE Trans. Electron. Devices **ED-25**, 1178 (1978).

[15]K. E. Peterson, Proc. IEEE **70**, 420 (1982).

[16]*VLSI Technology,* edited by S. M. Sze (McGraw-Hill, New York, 1983).

[17]I. Brodie and J. J. Muray, *Physics of Microfabrication* (Plenum, New York, 1982).

[18]R. Siegel and J. R. Howell, *Thermal Radiation Heat Transfer,* 2nd ed. (McGraw-Hill, New York, 1981).

[19]B. Gebhart, *Heat Transfer* (McGraw-Hill, New York, 1971).

[20]J. M. Elson, Phys. Rev. B **30**, 5460 (1984).

[21]P. W. Barber, R. K. Chang, and H. Massoudi, Phys. Rev. Lett. **50**, 997 (1983).

[22]*Surface Enhanced Raman Scattering,* edited by R. K. Chang and T. E. Furtak (Plenum, New York, 1982).

[23]C. J. Chen, H. H. Gilgen, and R. M. Osgood, Opt. Lett. **10**, 173 (1985).

[24]P. J. Hesketh, B. Gebhart, and J. N. Zemel, J. Heat Transfer (to be published).

[25]P. J. Hesketh, Ph. D. dissertation, University of Pennsylvania, Philadelphia, 1987.

[26]J. D. Jackson, *Classical Electrodynamics,* 2nd ed. (Wiley, New York, 1975).

[27]A. Borghesi, E. Bussoletti, L. Colangeli, V. Orofino, M. Guido, and S. Nunziante-Cesaro, Infrared Phys. **26**, 37 (1986).

[28]A. Borghesi, E. Bussoletti, and L. Colangeli, Astron. Astrophys. **142**, 225 (1985).

[29]R. W. Wood, Philos. Mag. **4**, 396 (1902).

[30]C. H. Liebert, in *Progress in Astronautics and Aeronautics: Thermophysics of Spacecraft and Planetary Bodies,* edited by G. B. Heller (Academic, New York, 1967), Vol. 20, p. 17.

[31]See the following paper (Ref. 2) for references to this literature and Table II for these values.

[32]E. D. Palik, *Handbook of Optical Constants of Solids* (Academic, New York, 1985).

[33]A. E. Siegman, *An Introduction to Lasers and Masers* (McGraw-Hill, New York, 1971), Chap. 11.

[34]J. Geist, J. Opt. Soc. Am. **62**, 602 (1972).

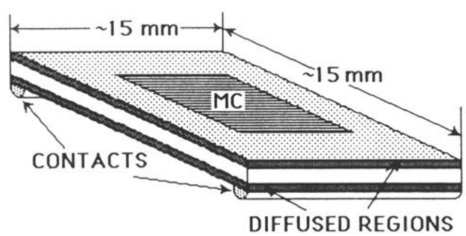

FIG. 1. Schematic drawing of the integrated microconfigured emittance sample.

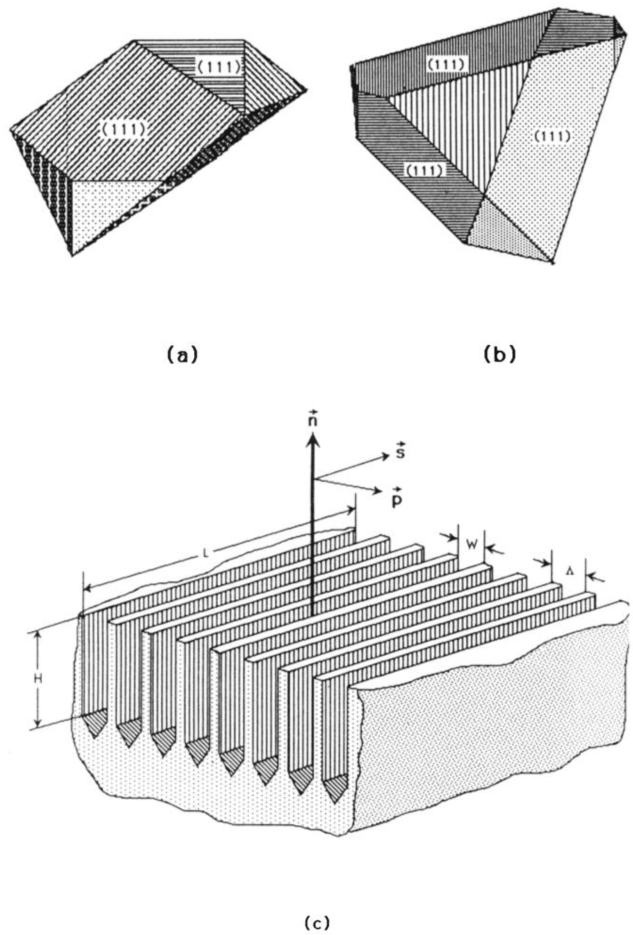

FIG. 2. Schematic drawings of three types of microconfigures surfaces. (a) "Hexagonal" cavities from square apertures; (b) schematic drawing of a rectangular "wedge" arising from rectangular apertures; (c) schematic drawing of the "deep" grating showing the orientation of the s- and p-polarization vectors relative to Λ. Also shown are the various characteristic geometric lengths defined in the text.